CEAS-GNC-2022-065

CEAS EuroGNC 2022
"Conference on Guidance, Navigation and Control"
3-5 May 2022 @ Technische Universität Berlin, Germany

Robust Observer-Based Space Launcher Control With Time-Varying Objectives

Felix Biertümpfel Research Associate, Chair of Flight Mechanics and Controls, Technische Universität Dresden, 01062, Dresden, Germany. felix.biertuempfel@tu-dresden.de

Julian Theis Control Engineer, Underwater Vehicles Engineering, ATLAS ELEKTRONIK GmbH, 28309 , Bremen, Germany. julian.theis@atlas-elektronik.com

Harald Pfifer Professor, Chair of Flight Mechanics and Controls, Technische Universität Dresden, 01062, Dresden, Germany. harald.pfifer@tu-dresden.de

ABSTRACT

This paper presents a novel approach for robust linear time-varying control design for space launchers. It allows the controller to explicitly respect the launcher's highly time-varying dynamics as well as changing control objectives along the ascent trajectory. The latter are readily incorporated via time-varying weighting functions in the mixed sensitivity synthesis. For a more traceable and effective control design a recently proposed weighting scheme is applied, which significantly reduces the controller tuning effort. The synthesis uses a novel observer-based finite horizon linear time-varying (LTV) synthesis approach. It provides a highly structured controller which is easy to implement and facilitates, for example, the incorporation of anti wind-up compensation. The approach is used to design a pitch controller for a small expendable launch vehicle in atmospheric ascent tracking the open-loop guidance reference signal.

Keywords: Linear Time-Varying Systems, Observer-Based Control, Space Launcher

1 Introduction

The atmospheric ascent of space launchers poses a formidable control problem. It requires the stabilization of an aerodynamically unstable system, the fulfillment of tight tracking constraints, load relief to fulfill stringent structural requirements as well as an optimal use of propellant. All these requirements must be fulfilled for constantly changing environmental conditions, rapidly decreasing mass, and thus, changing launcher dynamics. Besides, the launcher is subject to numerous external disturbances, such as wind turbulence.

State of the art control synthesis approaches do not explicitly respect the time-varying launcher dynamics in the controller synthesis. Most commonly, classic linear time-invariant (LTI) methods are applied to design and synthesize single controllers for frozen points in time along the trajectory. These controllers are then interpolated and scheduled with a measurable parameter such as the non-gravitational velocity. The resulting controllers are typically gain-scheduled proportional-integral-derivative (PID) controller [1, 2]. More recently, robust linear control methods such as mixed sensitivity H_∞ design [3] have been applied to the atmospheric ascent problem, see, e.g., [4]. However, classical gain scheduling for such controllers is in general complicated [5]. To resolve this matter, the structured H_∞ approach

[6] has been applied in e.g. [7]. The resulting controllers are more structured and easier to schedule. However, the design is still limited to frozen invariant points considered over infinite horizons. Therefore the approach fails to adequately cover the launchers time-varying dynamics. Moreover, for each point in time the controller has to be tuned separately. To account for the launchers varying dynamics and avoid the tuning of individual controller, linear parameter-varying (LPV) control has been applied to the ascent problem [8]. It uses the non-gravitational velocity as the scheduling parameter. However, the design is restricted to a relatively low number of grid points, due to the numerical and computational complexity of standard LPV control synthesis [9]. Therefore, the time varying-dynamics can only be covered coarsely. Also, LPV control considers infinite time horizons and, thus, neglects that the trajectory is finite. Thus, LTI and LPV syntheses fail to adequately cover the ascent problem, which is, in fact strictly time-dependent due to the pre-fedined trajectory. Therefore, finite horizon linear time-varying (LTV) control synthesis presents an alternative. The general suitability of finite horizon techniques to the launcher problem have been successfully demonstrated in [10, 11]. However, no application of robust finite horizon LTV methods for the launcher control problem can be found in literature.

The present paper proposes a novel approach to design a mixed-sensitivity finite horizon LTV controller for the ascent problem. It explicitly respects the launcher's time-varying dynamics in the synthesis. A representative LTV launcher model in atmospheric ascent is introduced in Section 3. The synthesis is conducted using the LTV equivalent of a recently proposed observer-based mixed sensitivity synthesis for LPV systems [12] introduced in Section 2. The synthesis procedure essentially requires the sequential solution of two unidirectionally coupled Riccati differential equations (RDEs). As these solutions scale better with the grid density as the LPV approach, a more accurate representation of the launcher dynamics over time is possible. Moreover, the resulting controller is highly structured making it particularly easy to implement. The control design applies a highly traceable weighting scheme first introduced in [13], which is presented in Section 3. The time-varying weights represent changing control objectives along the ascent trajectory, which are mainly imposed by the rapidly changing dynamic pressure.

The suitability of the approach is demonstrated via a nominal LTV analysis of the control design and a Monte Carlo simulation in Section 4. The Monte Carlo simulation is conducted over a large set of realistic wind turbulence as encountered by the launcher during ascent.

2 Background

2.1 Linear Time-Varying Systems

A finite horizon continuous LTV system $\mathbf{P}$ is defined as

$$\left[\begin{array}{c} \dot{x}(t) \\ \hline y(t) \end{array}\right] = \left[\begin{array}{c|c} A(t) & B(t) \\ \hline C(t) & D(t) \end{array}\right] \left[\begin{array}{c} x(t) \\ \hline u(t) \end{array}\right] \tag{1}$$

where $x(t) \in \mathbb{R}^{n_x}$ is the state vector, $u(t) \in \mathbb{R}^{n_u}$ the input vector, and $y(t) \in \mathbb{R}^{n_y}$ the output vector. Its system matrices are locally bounded continuous functions of time t. They are compatible size-wise to the corresponding vectors, e.g., $A(t) \in \mathbb{R}^{n_x \times n_x}$. The explicit time dependence will be omitted regularly to shorten the notation. The size of signals in this paper is measured by the $L_2[0,T]$ norm

$$\|u\|_{2[0,T]} = \left[\int_0^T u(t)^T u(t)\, dt\right]^{\frac{1}{2}}. \tag{2}$$

In the course of the paper, the notation $y = \mathbf{P}u$ is used to state the input-output map defined by the state space representation (1) for zero initial conditions. The performance of such a finite horizon LTV

input-output map can be quantified by its finite horizon induced $L_2[0,T]$ norm

$$\|\mathbf{P}\|_{2[0,T]} := \sup_{u\in L_2[0,T], u\neq 0, x(0)=0} \frac{\|y\|_{2[0,T]}}{\|u\|_{2[0,T]}}, \tag{3}$$

where $u \in L_2[0,T]$ implies $y \in L_2[0,T]$. An upper bound on $\|\mathbf{P}\|_{[0,T]}$ is provided by a generalization of the Bounded Real Lemma (BRL) as stated in the following theorem.

Theorem 1 ([14])**.** *Let* $\mathbf{P}$ *be an LTV system defined by (1). Given* $x(0)=0$*, if there exists a continuous differentiable, symmetric positive semi-definite matrix function* $Q(t), t\in[0,T]$ *such that* $Q(T)=0$ *and*

$$\dot{Q} = -QA - A^TQ + C^TC - (QB + C^TD)(D^TD - \gamma^2 I)^{-1}(D^TC + Q^TQ), \tag{4}$$

then γ *is an upper bound on the induced* $L_2[0,T]$ *gain of* $\mathbf{P}$*.*

Proof 1. *The proof is given in [14].*

2.2 Mixed Sensitivity Finite Horizon LTV Synthesis

This paper considers a standard unity feedback control loop with plant $\mathbf{P} = [\mathbf{P_d}\ \mathbf{P_u}]$ and controller $\mathbf{K}$. Both systems are finite horizon LTV systems. The plant has two inputs, namely the control input u and disturbance input d and a single output y. The plant's state space realization is

$$\left[\begin{array}{c}\dot{x}\\ \hline y\end{array}\right] = \left[\begin{array}{c|cc} A(t) & B_d(t) & B_u(t)\\ \hline C(t) & 0 & 0\end{array}\right] \left[\begin{array}{c} x\\ d\\ u\end{array}\right]. \tag{5}$$

The assumption that the plant model (5) is strictly proper is only made to simplify the notation and the following results can be generalized to non-strictly proper plants at the cost of more complicated notation. However, most engineering problems can be accurately represented by strictly proper models, for example, by including actuator dynamics in the model.

The considered four-block mixed sensitivity formulation characterizes performance as the finite horizon $L_2[0,T]$-norm of the weighted closed-loop system shown in Fig. 1. The corresponding optimal

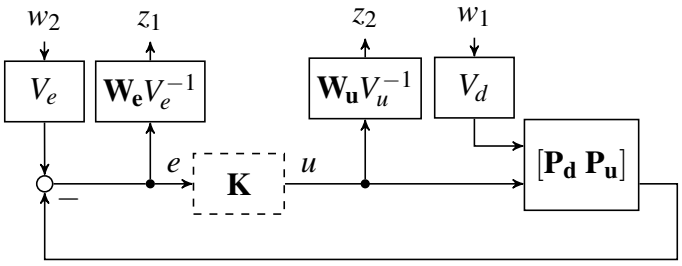

Fig. 1 Weighted four-block mixed sensitivity problem.

controller synthesis problem is

$$\min_K \left\| \left[\begin{array}{cc} \mathbf{W_e}V_e^{-1} & 0\\ 0 & \mathbf{W_u}V_u^{-1}\end{array}\right] \left[\begin{array}{cc} -\mathbf{SP_d} & \mathbf{S}\\ -\mathbf{KSP_d} & \mathbf{KS}\end{array}\right] \left[\begin{array}{cc} V_d & 0\\ 0 & V_e\end{array}\right] \right\|, \tag{6}$$

where $\mathbf{S} = (I + \mathbf{P_u K})^{-1}$ denotes the output sensitivity function [15]. Performance specifications are imposed through shaping filters $\mathbf{W_e}$ and $\mathbf{W_u}$ with state space realizations

$$\left[\begin{array}{c|c} \dot{\xi}_e & \\ \hline z_1 & \end{array}\right] = \left[\begin{array}{c|c} 0 & B_{We}(t) \\ \hline C_{We}(t) & D_{We}(t) \end{array}\right] \left[\begin{array}{c|c} \xi_e & \\ \hline \tilde{e} & \end{array}\right] \tag{7a}$$

$$\left[\begin{array}{c|c} \dot{\xi}_u & \\ \hline z_2 & \end{array}\right] = \left[\begin{array}{c|c} A_{Wu}(t) & B_{Wu}(t) \\ \hline C_{Wu}(t) & D_{Wu}(t) \end{array}\right] \left[\begin{array}{c|c} \xi_u & \\ \hline \tilde{u} & \end{array}\right]. \tag{7b}$$

A high gain in $\mathbf{W_e}$ enforces a sensitivity reduction and specifies tracking and disturbance rejection capabilities. An integrator in $\mathbf{W_e}$ enforces integral control. A high gain in $\mathbf{W_u}$ dictates a reduction in control effort. Hence, the weight $\mathbf{W_u}$ can dictate controller roll-off at high frequencies. The inputs to the dynamic weights $\mathbf{W_e}$ and $\mathbf{W_u}$ are a statically weighted control error $\tilde{e} = V_e^{-1} e$ and a statically weighted control effort $\tilde{u} = V_u^{-1} u$. The static time-varying weights V_e and V_u are tuning knobs that trade off tracking accuracy and control effort. They can be selected based on the maximum allowable errors (V_e) and maximum allowable inputs (V_u). Similarly, V_d is a tuning knob for disturbance rejection that can be chosen based on maximum expected disturbances. Thus, initial guesses are particularly easy. For details about this parametrization see [12, 13].

2.3 Structured Observer-Based LTV Control Synthesis

In [12] a novel observer based synthesis procedure for LPV systems is proposed that circumvents drawbacks of conventional LPV output feedback synthesis. The procedure uses the mixed sensitivity formulation (6) to solve for a structured observer-based LPV controller. It requires the separate solution of two semidefinite programs (SDPs), one for the observer and one for the state feedback problem and yields a highly structured controller. A strictly time-varying problem can be derived from the LPV case by considering only one specific parameter trajectory. In case of the launcher, this would be the precalculated ascent trajectory. The resulting time-dependent linear matrix inequalities can be reformulated using Schur's complement yielding two unidirectionally coupled RDEs. Assuming a finite time horizon these RDEs can be readily integrated. The resulting observer-based LTV controller $\mathbf{K}$ has the form:

$$\left[\begin{array}{c|c} \dot{\xi} & \\ \hline u & \end{array}\right] = \left[\begin{array}{c|c} A(t) + B(t)F(t) + L(t)C(t) & L(t) \\ \hline F(t) & 0 \end{array}\right] \left[\begin{array}{c|c} \xi & \\ \hline e & \end{array}\right], \tag{8}$$

where L is a time-varying observer gain and F is a time-varying state feedback gain. The structure of the controller is depicted in Fig. 2. Its dynamic part, the observer, consists of the three highlighted parts on the left. The following Theorem 2 formalizes the LTV case. To simplify notation, the weights and tuning knobs are chosen as $W_e = I$ and $W_u = I$ as well as $V_e = I$, V_u, and $V_d = I$, respectively.

Theorem 2 (Observer-Based Controller Synthesis)**.** *Consider an LTV system* (5)*. There exists an observer-based controller* $\mathbf{K}$ *defined by (8) such that* $\|\mathscr{F}(\mathbf{G},\mathbf{K})\| \leq \gamma$ *if the following two conditions hold.*

1) *There exists a continuously differentiable, symmetric positive semi-definite matrix function* $Z(t)$*,* $t \in [0,T]$ *such that* $Z(0) = 0$ *and*

$$\dot{Z} = AZ + ZA^T - ZC^T CZ + B_d B_d^T. \tag{9}$$

2) *There exists a continuously differentiable, symmetric positive semi-definite matrix function* $X(t)$*,* $t \in [0,T]$ *such that* $X(T) = 0$ *and*

$$\dot{X} = -\bar{A}^T X - X\bar{A} + X\bar{T}X + C^T \bar{U} C, \tag{10}$$

with $\bar{A} = A - \frac{1}{1-\gamma^2} ZC^T$, $\bar{T} = \frac{1}{1-\gamma^2} ZC^T CZ + B_u B_u^T$, *and* $\bar{U} = \frac{\gamma^2}{1-\gamma^2} C^T C$.

Proof. The given space limits the proof to a sketch. Essentially, the solvability of the RDE (9) guarantees the existence of a normalized left coprime factorization (see [16] for details) and provides the output injection gain $L = -ZC^T$. In the same way, the solvability of the RDE (10) guarantees the existence of a state feedback gain $F = -B_u^T X$. The co-isometric property of the LTV coprime factorization guarantees that the structured LTV synthesis provides the exact same induced $L_2[0,T]$-norm as the original LTV output feedback synthesis stated in, e.g., [17], [18], or [19]. □

The argumentation follows the proof in [12] for LPV systems to which the reader is referred for a discussion of the general case, including weights. The observer based approach avoids the two main short-comings of classical LTV output synthesis [18, 19], firstly, the solution of two RDEs coupled by a spectral radius condition, secondly, the synthesized controller's lack of structure.

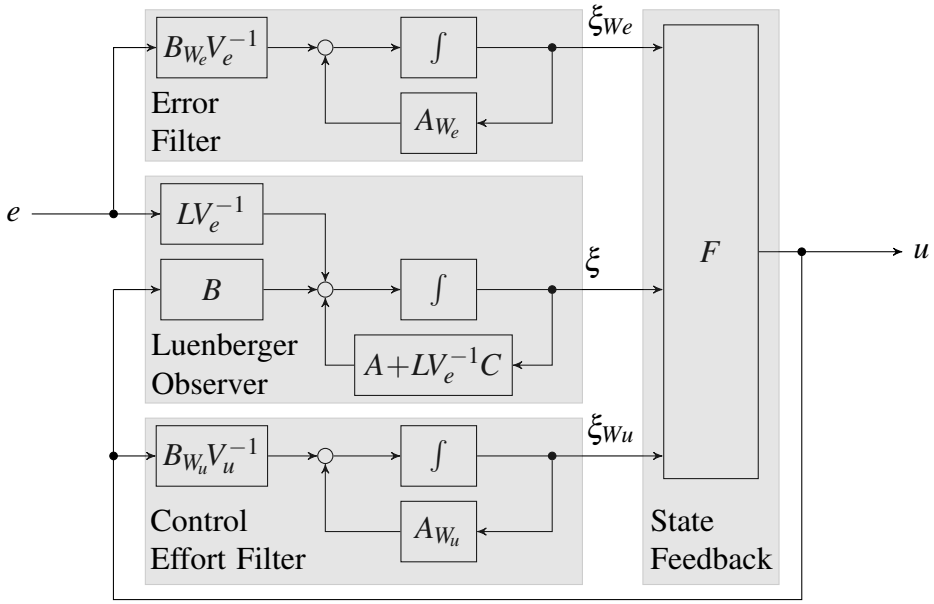

Fig. 2 Observer-based controller with weights

3 Space Launcher Control Design Problem

3.1 Model

A representative LTV model for a space launcher in atmospheric ascent is provided in [20]. It describes the first-stage rigid-body pitch dynamics of the Vanguard space launcher following a gravity turn trajectory. To include the effects of external wind disturbances in the control design, the model is extended with an additional input $\delta_{\dot{\alpha}}$ representing the additional wind-induced angle of attack. The corresponding LTV model is

$$\begin{bmatrix} \dot{\alpha}(t) \\ \dot{\theta}(t) \\ \dot{q}(t) \end{bmatrix} = \begin{bmatrix} \frac{Z_\alpha(t)}{m(t)v_{\mathrm{ref}}(t)} & \frac{-g\sin\theta_{\mathrm{ref}}}{v_{\mathrm{ref}}(t)} & 1 \\ 0 & 0 & 1 \\ \frac{M_\alpha(t)}{J_{yy}(t)} & 0 & \frac{M_q(t)}{J_{yy}(t)} \end{bmatrix} \begin{bmatrix} \alpha(t) \\ \theta(t) \\ q(t) \end{bmatrix} + \begin{bmatrix} \frac{T}{m(t)v_{\mathrm{ref}}(t)} & 1 \\ 0 & 0 \\ \frac{T\xi}{J_{yy}(t)} & 0 \end{bmatrix} \begin{bmatrix} \delta_\mu(t) \\ \delta_{\dot{\alpha}}(t) \end{bmatrix} \tag{11}$$

The states, which are also the system's output, are the angle of attack α, the pitch angle θ and the pitch rate q. They represent deviation values from the time-varying reference trajectory. The input δ_μ is the

corrective gimbal input rotating the thrust vector for attitude control. This signal is the output of a first order lag with $\omega = 50\text{rad}/s$ representing the gimbal dynamics, which are explicitly respected in the controller synthesis. The functions Z_α, M_α and M_q denote the aerodynamic stability derivatives. Their values along the trajectory are provided in [20] together with expressions for mass m and pitch inertia J_{yy} in dependence on t. The variables v_{ref} and θ_{ref} represent the reference velocity and pitch angle of the launcher along the trajectory. The values are given in [20] for the time interval $t \in [11.35, 146.35]$ with a step size of 2.7 s. The thrust T, the distance ξ of the center of gravity from the gimbal, as well as the gravitational acceleration g are constants.

3.2 Control Objective

The control design considers a time horizon from 15 s to 100 s after lift-off; the start and end point of the gravity turn maneuver. Fig. 3 shows the reference pitch angle value θ_{ref} along this trajectory segment as well as the value $\mu_\alpha = \frac{M_\alpha}{J_{yy}}$. The magnitude of μ_α is a measure for pitch stability. Larger values of μ_α indicate faster unstable dynamics posing in a more difficult control problem. Note that the launcher can

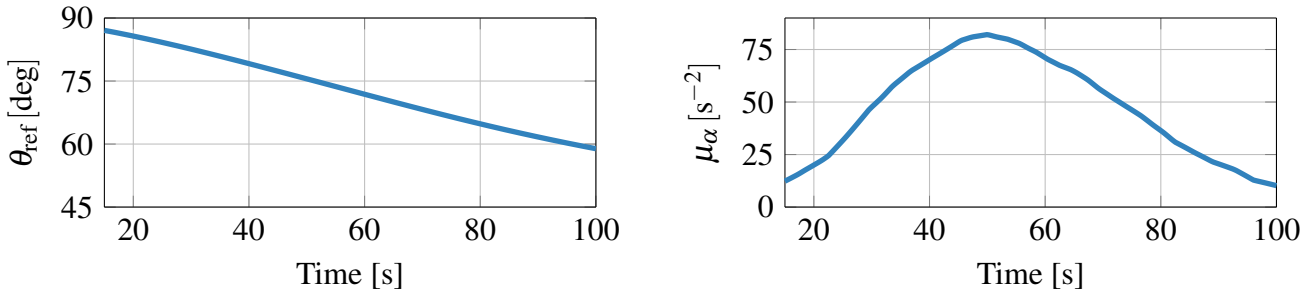

Fig. 3 Reference pitch angle θ_{ref} and pitch stiffness μ_α along the trajectory.

be considered perfectly rotationally symmetric. Furthermore, pitch and yaw dynamics can be considered decoupled in absence of a roll rate. Thus, it is sufficient to only design one controller for both motions. Typical pitch control objectives for space launcher during the atmospheric flight phase can be found in, e.g., [21, 22]. First, the controller must robustly stabilize the launcher along the ascent trajectory. However, considering the launcher as a finite horizon LTV problem nullifies classic stability arguments as linear systems have no finite escape time [23]. Hence, input-output norm analyses are more suitable for launch vehicle, see, e.g., [24]. Given a finite time horizon, the launcher dynamics at a frozen point along the trajectory can have poles in the right half-plane as long as no signal grows out of specified bounds, i.e. a specified norm gets too large. In principle, this characteristic can be exploited in the control design. An example is the so-called, load-minimum condition [25] for which, at a frozen point in time, the translational pole is in the right-half plane. The second important control objective is tracking performance under external disturbances such as atmospheric turbulence. The launcher must accurately follow the reference trajectory, i.e. θ_{ref}, ideally with zero error. The response time to commanded θ changes must be adequately fast, which requires sufficient controller bandwidth. Additionally, the transient response shall be constrained regarding maximum overshoot and maximum $\dot{\theta}$. At the same time, the aerodynamic loads on the launcher resulting from wind disturbances must be minimized to avoid structural failure. Thus, the induced aerodynamic angle of attack must be compatible with a general load specification, e.g., $Q\alpha < 150\,\text{kPaDeg}$. Note that $Q\alpha$ is simply the product of dynamic pressure Q and angle of attack α. It presents a common measure for the static aerodynamic load on launch vehicles. For the given launcher, this boundary corresponds to a maximum angle of attack of 4.56 deg for the maximum dynamic pressure $\bar{q}_{\max}$ of 32920 Pa at 50 s. Fig. 4 depicts the course of the dynamic pressure as well as the $\alpha_{\max}$ bound along the trajectory. The later is limited to a maximum of 10 deg. The second last requirement is the demanded gimbal actuation, which shall neither reach its deflection nor exceed the actuator bandwidth limit. The last requirement concerns the fuel consumption,

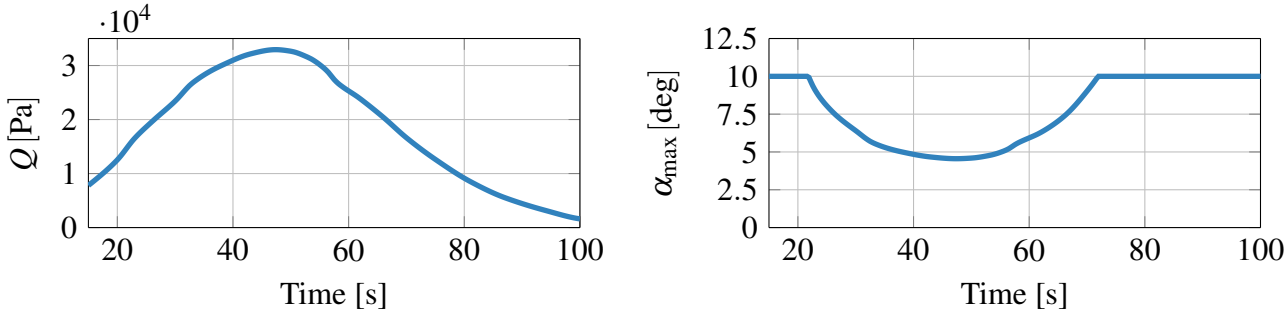

Fig. 4 Dynamic pressure Q along the trajectory and corresponding structural $\alpha_{\max}$ bound.

and therefore directly the cost-critical lift-off mass of the launcher. In order to minimize the required fuel consumption, the launcher shall not exceed a given cumulated commanded thrust deflection (the so-called consumption). A typical value for this type of launcher and trajectory segment is 20 deg · s.

However, the tracking and load relief objectives contradict each other, as tracking a given pitch angle under wind disturbance results in a significant load building up. Extremely tight control can result in a loss of the launch vehicle. Vice versa, minimizing $Q\alpha$ potentially results in a deviation from the trajectory too large to correct and, thus, likewise in mission failure. It is thus clear, that control objectives for launch vehicle, require noticeable trade-offs which also change over time during the ascent. Hence, time-varying control presents is beneficial to not only account for the time-varying dynamics, but also the time-dependent control objectives of launch vehicles.

3.3 Weighting Scheme and Control Synthesis

Based on the control objectives and the expected disturbances, the dynamic weights $\mathbf{W}_\mathrm{e}$ and $\mathbf{W}_\mathrm{u}$, as well as static weights V_e, V_u, and V_d are selected. Following the formulation and recommendations in [13], the weighting filter $\mathbf{W}_\mathrm{e}$ affects the disturbance sensitivity. Therefore, it describes the requirements on sensitivity. As a θ tracker shall be designed, integral behavior in the θ channel up to 12.5 rad/s and a magnitude of 0.5 beyond is selected. To account for the increasing dynamic pressure and slow down the tracking, the desired bandwidth ω_bw is gradually reduced to as low as 6 rad/s in the area of maximum dynamic pressure (40 s-60 s). The design aims for a closed-loop bandwidth, which is at least five-times faster than the most unstable pole (1.14 rad/s at 50 s into the ascent). It also separates the controller bandwidth by a factor of at least four from the gimbal's bandwidth. However, the gimbal dynamics remain a crucial part of the synthesis model to increase robustness towards phase delays. A frequency-independent constant weighting of 0.5 is chosen for the remaining feedback signals, namely α and q. The weighting filter $\mathbf{W}_\mathrm{u}$ determines the control sensitivity and represents the actuator limitations as well as robustness requirements. It is selected with unit gain up to 25 rad/s, i.e., half the gimbal bandwidth. Beyond 25 rad/s, differentiating behavior is selected to enforce controller roll-off.

Afterwards, the tuning knobs are selected, which are based on the control objectives in Section 3.2. The static weight V_e represents the maximum command value for tracked outputs and balances the three output errors. It is chosen time-varying, given the changing requirements along the trajectory. At the beginning and end of the trajectory pitch tracking is prioritized over load relief. Hence, a small value for V_e in the θ channel (V_{e_θ}) and larger values in the α (V_{e_α}) and q (V_{e_q}) channels are chosen. The latter influences the transient behavior, which is allowed to be faster in the low dynamic pressure regions. Tab. 1 presents the numerical values chosen for the elements of V_e. Cubic Hermite interpolating polynomials are used to interpolate the points in-between the grid points, to assure smoothness. Fig. 5 depicts the course of the weights along the trajectory. The V_{e_α} values are selected based on the $\alpha_{\max}$ bound in Fig. 4 with a safety margin. For the other two channels, values corresponding to the allowed errors in [21, 22] are selected. To assign the available control action relative to the previously specified maximum errors,

Table 1 Values of the weights along the trajectory

	15 s	30 s	40 s	50 s	60 s	80 s	100 s
ω_{bw} [rad/s]	12	10	8	6	8	10	12
V_{e_α} [deg]	10	6	4.5	4.5	6	10	10
V_{e_θ} [deg]	0.25	0.5	1	1	0.5	0.25	0.25
V_{e_q} [deg/s]	1	0.75	0.5	0.4	0.5	0.75	1
V_u [deg]	10	8.5	7.5	6.0	7.5	8.5	10
V_d [deg/s]	2.5	2	0.5	0.1	0.5	2.0	2.5

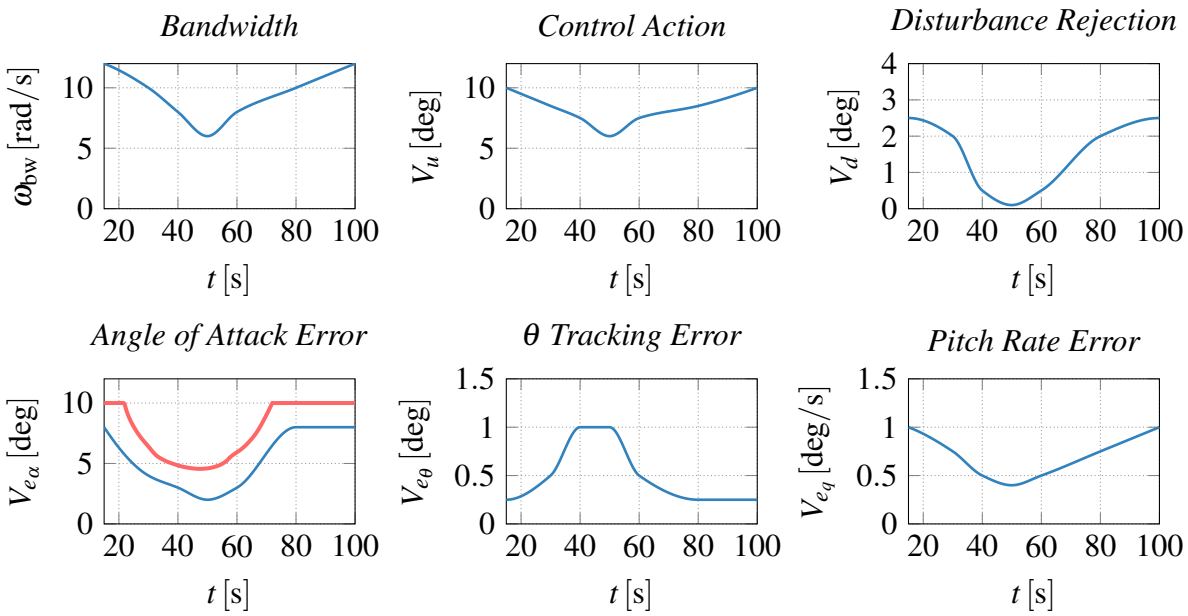

Fig. 5 Tuning parameter along the trajectory: Selected Value (——), Control Objective (——)

the weight V_u is used. Its values are based on the gimbal dynamics, typical deflection limits of thrust vector control system, and to reduce the consumption. For the considered launcher, a value of 6 deg in the high pressure region is chosen and 10 deg elsewhere (see Tab. 1 for details). The selection also aims for a reduction of the control effort in the high pressure region for load relief purposes. The ratio V_e/V_d determines the trade-off between tracking performance and disturbance rejection. Hence, disturbance rejection is favored in the range of maximum dynamic pressure. The selected values for V_d are shown in Tab. 1.

Using these weights, the observer synthesis and calculation of the output injection gain L can be performed. It requires solving a scaled version of the RDE (9), which can be readily derived following the explanations in [12]. The RDE is solved using the Matlab solver `ODE15s` [26], suitable for stiff differential equations, a typical property of RDEs, see e.g. [27]. The solution takes 0.09 s on a standard desktop PC. Next, the state feedback synthesis is conducted, using L from the previous step. The calculated feedback gain minimizes the $L_2[0,T]$ of the output feedback problem. Again, `ODE15s` in Matlab is used to solve the RDE. A bisection calculates the minimal feasible γ as $\gamma = 3.75$ and takes 3.51 s. Thus, the complete controller synthesis requires approximately 4.2 s. Finally, the finite horizon LTV controller is formed from the feasible solutions of the RDEs, the plant state space matrices and the weighting filters

following Fig. 2. The low amount of time for synthesis allows for a fast tuning process. Compared to the LPV approaches, see e.g. [8], LTV synthesis facilitates significantly higher grid densities. Thus, significantly more accurate representation of the launcher dynamics are possible in the synthesis.

4 Results

First, an LTV simulation of the resulting closed-loop model is conducted in Matlab. The closed loop is exited by an external wind disturbance. The wind disturbance consists of a Gaussian white noise signal with a sampling time of 0.5 s and variance 1, and a static mean value of zero. It induces an α disturbance on the launcher shown in Fig. 6. The control signal counteracts the disturbance and keeps the deviation θ close to zero for the whole ascent. The required gimbal deflection remains below the saturation limit. Thus, the controller displays excellent disturbance rejection. It is particularly noteworthy that no variation in performance is visible, although the unstable dynamics of the launcher vary significantly over time (see Fig. 3). In conclusion, the proposed control design approach proofs suitable for a highly time-varying problem.

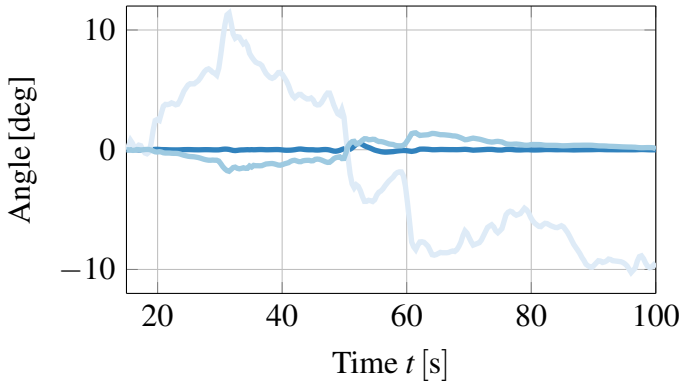

Fig. 6 Nominal performance results of the LTV simulation: α disturbance (——), θ deviation (——), control signal (——)

After confirming the nominal performance of the controller, a Monte Carlo simulation over a large set of realistic wind disturbances is conducted. The analyzed wind disturbance w shall resemble Dryden turbulence profiles, which are frequently used in aerospace certification [28]. In the Monte Carlo simulation the Dryden filter G_w for vertical turbulence

$$\begin{aligned} \dot{x}_w(t) &= \begin{bmatrix} 0 & 1 \\ -\left(\frac{v_{\mathrm{ref}}(t)}{L_w(t)}\right)^2 & -2\frac{v_{\mathrm{ref}}(t)}{L_w(t)} \end{bmatrix} x_w(t) + \begin{bmatrix} 0 \\ \left(\frac{v_{\mathrm{ref}}(t)}{L(t)}\right)^2 \end{bmatrix} n_w(t) \\ w(t) &= \begin{bmatrix} \sigma(t)\sqrt{\frac{L_w(t)}{\pi v_{\mathrm{ref}}(t)}} & \sigma(t)\frac{L_w(t)}{v_{\mathrm{ref}}(t)}\sqrt{\frac{3L_w(t)}{\pi v_{\mathrm{ref}}(t)}} \end{bmatrix} x_w(t), \end{aligned} \tag{12}$$

with white noise input n_w is implemented to generate w. The filter G_w shapes signals with constant power spectral density (PSD) into turbulence profiles statistically matching real turbulence. In (12), v_{ref} is the velocity of the launcher, σ is the turbulence intensity and L_w is the turbulence scale length. Note that σ's as well as L_w's altitude dependence convert to a strict time dependency along the design trajectory. A moderate turbulence intensity according to MIL-F-8785C is chosen.

Using this type of explicit wind disturbance requires a slight change of the Launcher LTV model's input channel from $\dot{\alpha}$ to a wind velocity disturbance w of unit $[\mathrm{m/s}]$. Here the wind disturbance is approximated as $\alpha_w \approx \frac{v_w}{v_d}$. Hence, in (11) the second column of the B and D matrices changes to $\left[\frac{Z_\alpha(t)}{m(t)v_{\mathrm{ref}}(t)^2}\ 0\ \frac{M_\alpha(t)}{J_{yy}(t)v_{\mathrm{ref}}(t)}\right]^T$ and $\left[\frac{1}{v_{\mathrm{ref}}}\ 0\ 0\right]^T$, respectively.

A total of 10000 unique wind signals w are evaluated, whose PSDs compare to real turbulence. Fig. 7 depicts the wind signals as well as the resulting values of α, θ, and the commanded gimbal deflection u_{cmd}. Focusing first on the induced angle of attack, the limit value α_{max} is never violated. A maximum absolute value of 8.27 deg at 21.45 s was identified, which is a factor of 1.2 lower than the local α_{max}. In the high pressure region, α never exceeds an absolute value of 3.3 deg and thus remains well below the threshold. During the whole atmospheric ascent the tracking error θ remains small with the maximum absolute deviation of 0.19 deg occurring in the high dynamic pressure region at 49.22s. In the low pressure region, θ never exceeds 0.17 deg. The commanded control effort remains small over the whole trajectory, with a maximum absolute gimbal deflection of 0.83 deg at 30.91 s. It remains well below the saturation limit of 10 deg Fig. 8 shows a distribution of the calculated consumptions, i.e., the cumulative control effort along the trajectory. The maximum consumption is 7.39 deg, which is almost three times lower than the threshold of 20 deg. The behavior of the θ, α, and control effort signals clearly reflect the influence of the time-varying control design. At the beginning of the ascent where dynamic pressure is low, tracking is favored over load relief. In the middle of the ascent, load relief is favored resulting in less stringent tracking and, thus, reduced control effort and smaller induced angles of attack. At the end

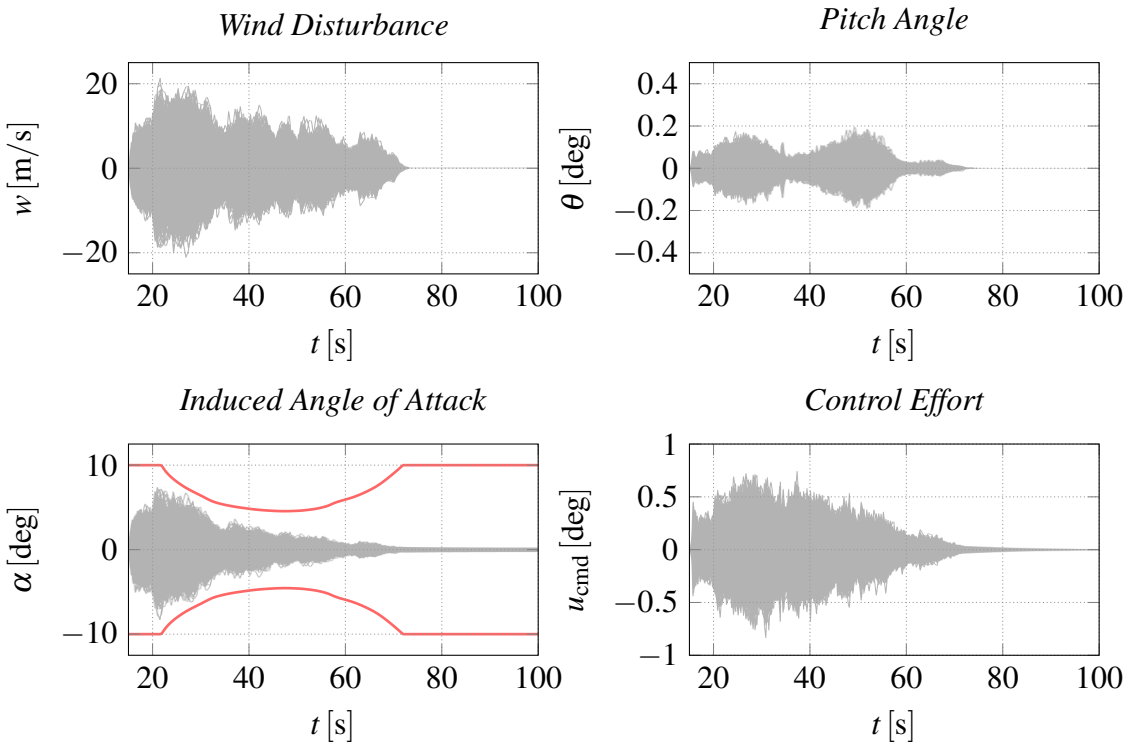

Fig. 7 LTV Monte Carlo Simulation Results: Simulation Result (– – –), Limit Value (——)

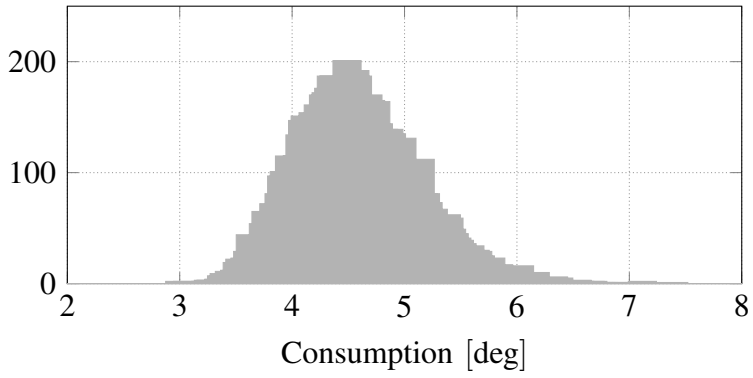

Fig. 8 Histogram of consumption (– – –) obtained from 10000 Monte Carlo Simulations

of the trajectory the tracking becomes tighter again. However, the wind disturbance significantly starts to decay in the corresponding altitude band. Hence, the induced angles of attack reduce as well.

5 Conclusion

A finite horizon LTV design for a space launcher in atmospheric ascent is presented. The synthesis explicitly includes the launcher's time-varying dynamics as well as the variation of the control objectives along the ascent trajectory. The applied time-varying weighting scheme results in a particularly traceable tuning procedure strictly based on the control objectives and expected disturbances. A novel synthesis procedure for finite horizon LTV systems is applied, which yields a highly structured controller. The concluding Monte Carlo simulation over a large set of realistic wind disturbances demonstrated the suitability of LTV control for the ascent problem.

Acknowledgments

This work has been partially funded by ESA under the OSIP Co-Funded Research Program contract number 4000135/85/21/NL/GL/my.

References

[1] B. Clement, G. Duc, and S. Mauffrey. Aerospace launch vehicle control: a gain scheduling approach. *Control Engineering Practice*, 13(3):333–347, 2005. DOI: 10.1016/j.conengprac.2003.12.013.

[2] A. G. Silva and W. C. Leite Filho. Launch vehicle attitude control system using PD plus phase lag. *IFAC Proc. Vol.*, 46(19):48–53, 2013. DOI: 10.3182/20130902-5-de-2040.00110.

[3] H. Kwakernaak. Mixed sensitivity design. *IFAC Proc. Vol.*, 35(1):61–66, 2002. DOI: 10.3182/20020721-6-es-1901.01236.

[4] D. Sánchez de la Llana, S. Bennani, I. Cruciani, and J. Aranda. H-infinity control of the VEGA launch vehicle first stage in presence of roll. *IFAC Proc. Vol.*, 46(19):54–59, 2013. DOI: 10.3182/20130902-5-de-2040.00039.

[5] R. A. Hyde. An H(infinity) loop-shaping design for the VAAC harrier. In Roger W. Pratt, editor, *Fligh Control Systems*, pages 348–373. American Institute of Aeronautics and Astronautics, 2000. DOI: 10.2514/5.9781600866555.0348.0373.

[6] P. Apkarian and D. Noll. Nonsmooth H∞ synthesis. *IEEE Trans. Automat. Control*, 51(1):71–86, 2006. DOI: 10.1109/tac.2005.860290.

[7] M. Ganet-Schoeller and J. Desmariaux. Structured H∞ synthesis for flexible launcher control. *IFAC-PapersOnLine*, 49(17):450–455, 2016. DOI: 10.1016/j.ifacol.2016.09.077.

[8] D. Navarro-Tapia, A. Marcos, and S. Bennani. The VEGA launcher atmospheric control problem: A case for linear parameter-varying synthesis. *J. of the Franklin Inst.*, 2021. DOI: 10.1016/j.jfranklin.2021.07.057.

[9] F. Wu, X. H. Yang, A. Packard, and G. Becker. Induced L2-norm control for LPV systems with bounded parameter variation rates. *Int. J. Robust and Nonlinear Control*, 6(9-10):983–998, 1996.

[10] F. Biertümpfel, H. Pifer, and S. Bennani. Finite horizon worst case analysis of launch vehicles. *IFAC-PapersOnLine*, 52(12):31–36, 2019. DOI: 10.1016/j.ifacol.2019.11.065.

[11] F. Biertümpfel, S. Bennani, and H. Pfifer. Time-varying robustness analysis of launch vehicles under thrust perturbations. *Advanded Control For Applications*, 2021. DOI: 10.1002/adc2.93.

[12] J. Theis and H. Pfifer. Observer-based synthesis of linear parameter-varying mixed sensitivity controllers. *Int. J. Robust Nonlinear Control*, 30(13):5021–5039, 2020. DOI: 10.1002/rnc.5038.

[13] J. Theis, H. Pfifer, and P. Seiler. Robust modal damping control for active flutter suppression. *J. Guidance, Control, Dynamics*, 43(6):1056–1068, 2020. DOI: 10.2514/1.g004846.

[14] G. Tadmor. Input/output norms in general linear systems. *Int. J. Control*, 51(4):911–921, 1990. DOI: 10.1080/00207179008934104.

[15] M. Green and D. J. N. Limebeer. *Linear Robust Control*. Prentice-Hall, Inc., Upper Saddle River, NJ, USA, 1995.

[16] R. Ravi, A.M. Pascoal, and P.P. Khargonekar. Normalized coprime factorizations for linear time-varying systems. *Systems & Control Letters*, 18(6):455–465, 1992. DOI: 10.1016/0167-6911(92)90050-3.

[17] P. P. Khargonekar, K. M. Nagpal, and K. R. Poolla. H_∞ control with transients. *SIAM J. Control Optim.*, 29(6):1373–1393, 1991. DOI: 10.1137/0329070.

[18] D. J. N. Limebeer, B. D. O. Anderson, P. P. Khargonekar, and Michael Green. A game theoretic approach to $\mathscr{H}^\infty$ control for time-varying systems. *SIAM J. Control Optim.*, 30(2):262–283, 1992. DOI: 10.1137/0330017.

[19] R.T. O'Brien and P.A. Iglesias. Robust controller design for linear, time-varying systems. *Eur. J. Control*, 5(2-4):222–241, 1999. DOI: 10.1016/s0947-3580(99)70157-3.

[20] A. Tewari. *Automatic Control of Atmospheric and Space Flight Vehicles: Design and Analysis with Matlab and Simulink*. Springer, 2011.

[21] M. Ganet and M. Ducamp. LPV control for flexible launcher. In *AIAA Guidance, Navigation, and Control Conference*, 2010. DOI: 10.2514/6.2010-8193.

[22] P. Simplicio, S. Bennani, A. Marcos, C. Roux, and X. Lefort. Structured singular-value analysis of the vega launcher in atmospheric flight. *J. Guidance, Control, Dynamics*, 39(6):1342–1355, 2016. DOI: 10.2514/1.g000335.

[23] J J. Slotine and W. Li. *Applied nonlinear control*. Prentice Hall, Englewood Cliffs, N.J, 1991.

[24] F. Biertümpfel and H. Pfifer. Worst case gain computation of linear time-varying systems over a finite horizon. In *2018 IEEE Conference on Control Technology and Applications*, 2018. DOI: 10.1109/ccta.2018.8511591.

[25] A. L. Greensite. Analysis and design of space vehicle flight control systems. volume VII - attitude control during launch. Technical report, NASA Marshall Space Flight Center; Huntsville, AL, 1967.

[26] MATLAB. *R2020b*. The MathWorks Inc., Natick, Massachusetts, 2020.

[27] Hisham Abou-Kandil, Gerhard Freiling, Vlad Ionescu, and Gerhard Jank. *Matrix Riccati Equations in Control and Systems Theory*. Birkhäuser Basel, 2003. DOI: 10.1007/978-3-0348-8081-7.

[28] F. M. Hoblit. *Gust Loads on Aircraft: Concepts and Applications*. American Institute of Aeronautics and Astronautics, 1988. DOI: 10.2514/4.861888.